Available online at www.sciencedirect.com

ScienceDirect

Transportation Research Procedia 7 (2015) 631 – 650

Transportation Research Procedia

www.elsevier.com/locate/procedia

21st International Symposium on Transportation and Traffic Theory, ISTTT21 2015, 5-7 August 2015, Kobe, Japan

Macroscopic Traffic Dynamics with Heterogeneous Route Patterns

Ludovic Leclercq[a,b,*], Céline Parzani[a], Victor L. Knoop[b], Jennifer Amourette[a], Serge P. Hoogendoorn[b]

[a]*COSYS-LICIT, IFSTTAR, ENTPE, Université de Lyon, France*

[b]*Department of Transport and Planning, Faculty of Civil Engineering and Geosciences, Delft University of Technology, the Netherlands*

Abstract

This paper investigates at an aggregated (macroscopic) scale the effects of route patterns on a road network. Four main variables are considered: the production, the mean speed, the outflow and the mean travel distance. First, a simple network with heterogeneous travel distances between origins and destinations is studied by simulation. It appears that the mean travel distance is not only very sensitive to the changes in the origin-destination (OD) matrix but also to the internal traffic conditions within the network. When this distance is assumed constant as usual in the literature, significant errors may appear when estimating the outflow at the network perimeter. The OD matrix also modifies the shape of the macroscopic fundamental diagram (MFD) to a lesser extend. Second, a new modelling framework is proposed to account for multiple macroscopic routes within reservoirs (spatial aggregates of road network) in the context of MFD simulation. In contrast to existing works, partial accumulations are defined per route and traffic waves are tracked at this level. This leads to a better representation of wave propagation between the reservoir frontiers. A Godunov scheme is combined to a HLL Riemann approximate solver in order to derive the model numerical solutions. The accuracy of the resulting scheme is assessed for several simple cases. The new framework is similar to some multiclass models that have been elaborated in the context of link traffic dynamics.

Selection and peer-review under responsibility of Kobe University

Keywords: network fundamental diagram; macroscopic fundamental diagram; traffic dynamics; travel production; mean travel distance; mean spatial speed; route choices; macroscopic traffic simulation; macroscopic origin-destination.

* Corresponding author. Tel: +33 4 72047716

E-mail address: ludovic.leclercq@entpe.fr

Selection and peer-review under responsibility of Kobe University

doi:10.1016/j.trpro.2015.06.033

1. Introduction

Mitigating congestion in large-scale cities remains a large challenge for traffic managers. Classically, traffic management systems in an urban context resort to optimizing traffic signals and route guidance. Efficient management schemes exist for traffic management at local and intermediate urban scales, e.g. SCOOT (Hunt *et al.*, 1983), SCATS (Lowrie, 1982) and TUC (Kouvelas *et al.*, 2011) but they hardly face the complexity of large urban areas. Recently, innovative strategies have been introduced based on perimeter flow control for urban sub-regions. For example, the city of Zürich (Switzerland) has implemented a control access strategy (Züritraffic) to maintain a sufficient level of service in the inner center. The implemented control scheme corresponds to pre-determined signal settings at the perimeter that are applied depending on the feedback from loops within the region. Such a strategy is appealing because it permits to revisit traffic signal control for urban networks by introducing a two-layer approach. The first level is a perimeter and boundary flow control that mitigates the level of congestion between different regions in order to improve the system efficiency at an aggregate level. The second layer corresponds to classical local traffic controls that smooth traffic movements within the regions.

A powerful tool to investigate aggregate traffic behavior is the concept of Macroscopic Fundamental Diagram (MFD). This concept provides for network regions a well-defined relation between space-mean flow and density (or vehicle accumulation). The idea of an MFD belongs to Godfrey (1969) and similar approaches were introduced later by Herman and Prigogine (1979), Mahmassani *et al.* (1984, 1987) and Daganzo (2007). The verification of its existence with dynamic features has been firstly realized using loops data from downtown Yokohama (Geroliminis and Daganzo, 2007; 2008). This concept has already been utilized to numerically experiment simple perimeter flow control policies in homogeneous networks (Daganzo, 2007; Keyvan-Ekbatani *et al.*, 2012; Geroliminis *et al.*, 2013; Aboudolas and Geroliminis, 2013; Knoop and Hoogendoorn, 2014; 2015). Most of the papers use the MFD concept to simulate the dynamic evolution of the vehicle accumulation within the reservoirs. This corresponds to a new class of traffic simulators that work with an aggregate description of the urban network but keep a dynamic description of congestion spreading.

Despite the recent findings for the existence of MFD with low scatter, such curves cannot be a universal law because network topology, origin-destination matrix and route choices might affect the shape and scatter under different cases. For example, (Geroliminis and Sun, 2011; Mazloumian *et al.*, 2010; Knoop *et al.*, 2013) have identified that the uneven spatial distributions of vehicle density in the network lead to traffic states that are well below the upper bound of an MFD and much too scattered to line along an MFD. (Leclercq and Geroliminis, 2013) has also shown that flow distributions associated to driver route choices may influence the MFD shape for a simple parallel network. It then appears that the demand pattern and the route allocation within a reservoir modify the overall performance of an urban network. A key element is that non-Manhattan network topology with unbalanced origin-destination tables and route choices clearly lead to non-homogeneous network loadings. Notably, traffic flows between the different parts of the reservoir perimeter may be unevenly distributed. A first solution to circumvent this drawback and to resort again to well-defined MFD is network partitioning (Ji and Geroliminis, 2012). In each sub-reservoir, traffic conditions may then be homogenous enough to exhibit a MFD. However, this does not solve all the problems because travel distances within sub-reservoirs can remain highly distributed depending on the reservoir shape and the entry and exit points for vehicles.

This paper proposes to investigate the relations between route patterns within a network and the related aggregate traffic dynamics. The main contributions are twofold: first, simulation results on an idealized and simple network provide insights on how main aggregated traffic variables are influenced by the external demand (OD matrix) and the internal traffic conditions. A particular attention is paid to the mean travel distance. It appears that this variable is far from constant when a large set of different and heterogeneous network loadings is considered. Second, a new aggregate dynamic traffic model will be proposed. This model splits the reservoir perimeter into different macroscopic origins and destinations in order to define aggregate internal routes. Thus, the travel distance is no longer uniform but can be defined for each internal route. This provides an insightful framework to monitor the heterogeneities due to route patterns within a reservoir without requiring to track traffic conditions in all network links. Furthermore, the model can more easily handle changes in the MFD due to the changes in the OD. This should pave the way to more accurate aggregate simulators and a better account for heterogeneous network loadings.

The remaining of the paper is organized as follow: Section 2 presents the results of the simulation study and highlights how the OD matrix and the internal traffic conditions impact the mean travel distance and the MFD shape within a reservoir. Section 3 describes the new multi-routes macroscopic model, investigates its properties and proposes a simple and efficient numerical scheme to simulate the in- and outflows. Section 4 provides a discussion and pinpoints some potentially important applications of this new framework.

2. Influence of heterogeneous route patterns on macroscopic traffic dynamics

This section aims to highlight some not well-known relations between the internal heterogeneities, the loadings and the macroscopic characteristics of a network. We chose to work with a small and simple network design because our goal is not to get final conclusions on the impacts in practice but to gain insights that could pave the way for further investigations. The results justify the need for a refined modeling framework that explicitly account for internal routes even at an aggregated level.

2.1. Simulation settings

We consider here a network with 4 origins and 6 destinations, see Fig. 1a. All links are unidirectional. Vertical link are from north to south while horizontal links are from west to east. Lengths are provided in Fig. 1a. Origins are gathered in a single macroscopic origin O_1 while destinations are split into two macroscopic destinations D_1 and D_2. The macroscopic route R_1 corresponds to travels from north to east, $O_1 \rightarrow D_1$, while R_2 gathers travels from north to south, $O_1 \rightarrow D_2$. This network has been specifically designed to have unbalanced behaviors between the two macroscopic routes with shorter travel distances on R_2. Heterogeneous route patterns are then observed.

Traffic dynamics within the network is simulated using a mesoscopic LWR model (Leclercq and Becarie, 2012). The simulator provides the time when each vehicle crosses the internal link boundaries. The fundamental diagram is triangular with same parameters for all links: free-flow speed, u=25 m/s, wave speed, w=5 m/s and jam density κ=0.2 veh/m. Traffic signals are implemented at all intersections with identical settings: green time, 30 s, cycle, 60 s, null offset. The demand distribution is always uniform from a local origin to all the reachable local destinations related to a given macroscopic destination. For example, the demand is equally split between $o_{1,1}$ and $d_{1,1}$-$d_{1,2}$ for D_1 and between $d_{2,1}$-$d_{2,2}$-$d_{2,3}$-$d_{2,4}$ for D_2. Let τ be the fraction of total demand on route R_1 ($O_1 \rightarrow D_1$). τ values are taken from 0 to 100% to cover a large diversity of OD matrix with different macroscopic route distributions. Internal route choices are driven by a traffic assignment component that implements the Wardrop's definition for user equilibrium (Wardrop, 1952).

A large variety of network loadings is applied to this network to reproduce either free-flow or congested situations. A network loading corresponds to a random draw for the total demand in O_1 and all the capacities at destinations. The total demand is uniformly split among the four local origins. Free-flow situations are observed when all capacities at destinations are set to the maximum values. Low capacity values at destinations mimic congestions that spillback from outside of the network. The simulation is run until a (quasi-) stationary situation is reached, i.e. when the absolute gap between the total inflow and outflow is below 5% over a running period of 20 minutes. Averaging in- and outflows over a 20 min period avoids local fluctuations due to the traffic signals. A strict equality between in- and outflows is never achieved because the simulator uses integer vehicle numbers and because heavy congested situations may not be fully stable. This is the reason for the 5% threshold.

Then, the macroscopic variables are calculated over a period of T=20 min within the reservoir defined by the green area in Fig. 1a. Practically, the simulation is run as long as necessary but only the last 20 minutes are considered. The macroscopic variables are:

- the number of vehicles (accumulation), n;
- the travel production, P;
- the mean speed, V;
- the outflow, Q;
- the mean travel distance, L.

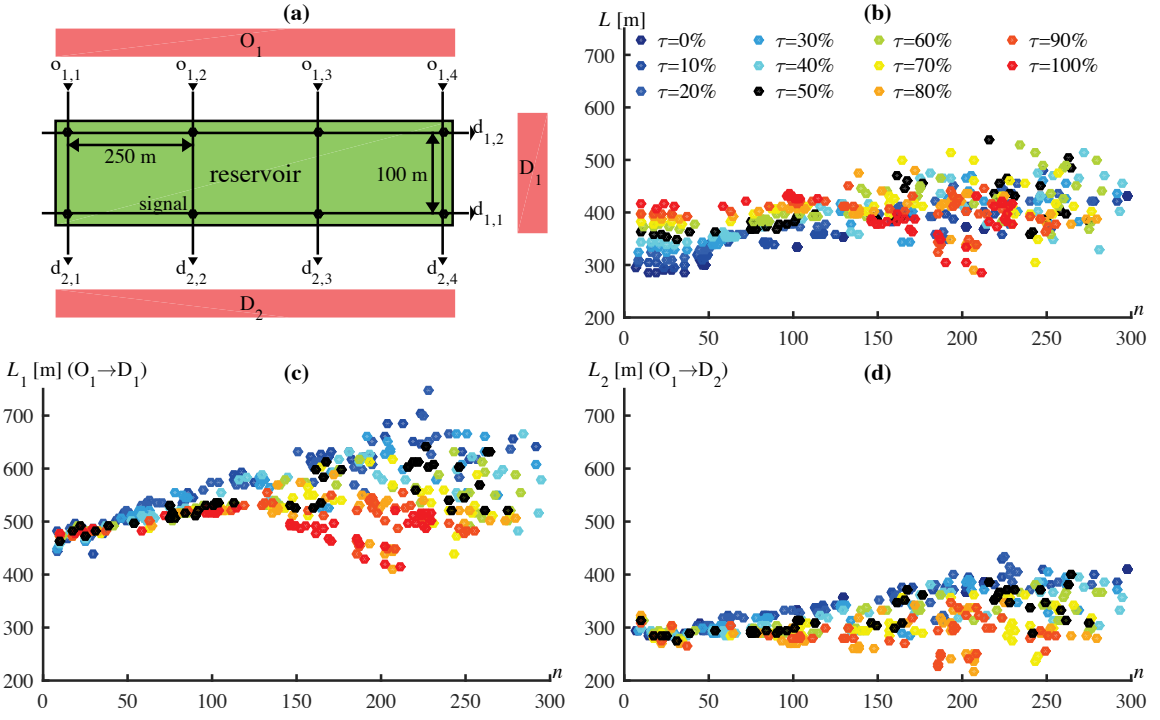

Fig. 1. (a) Sketch of the network; Influence of the OD matrix and the accumulation on (b) the global mean travel distance L, (c) the mean travel distance L_1 between O_1 and D_1, and (d) the mean travel distance L_2 between O_1 and D_2.

The accumulation n is calculated as the total travel time for all vehicles during the T period divided by T. The travel production P corresponds to the total travel distance for all vehicles also divided by T. The mean speed V is equal to P/n. The outflow is simply measured at exits. Finally, the mean travel distance L is given by P/Q (Daganzo, 2007). Such variables can also be determined for specific macroscopic routes by only considering vehicles whose macroscopic destinations are 1 or 2. In that case, a subscript (1 or 2) is added to the variable name.

2.2. Sensitivity of the mean travel distance to the OD matrix and the internal traffic conditions

Let first investigate the mean travel distance L with respect to τ and n for all the simulation runs, see Fig. 1b. It immediately appears that L depends on both the flow distribution between the macroscopic destinations, i.e. τ and the traffic conditions within the network, i.e. n. The results for all runs are very scattered: the standard deviation for L is equal to 56 m while the mean is equal to 421 m. For most τ values, L seems to increase with n ($\tau < 60\%$). For other values, no clear trend appears or L may also decrease. Note that n is not necessarily sufficient to fully characterize the network internal traffic conditions because its distribution over links can be more or less heterogeneous. Fig. 3d presents the standard deviation s_k of the density over links with respect to n. It appears that the higher n is, the more heterogeneous traffic conditions over the network are. This figure also shows that very different loadings in terms of heterogeneity can be achieved with same n when the network is heavily congested (n>180). This may be a second source of scattering for L when n is high.

Free-flow conditions are observed in this network for n values below approximately 90 veh when τ=100% to below 40 veh when τ=0%. L appears to be nearly constant in free-flow for a given τ values but varies from 300 m to 420 m when τ increases from 0 to 100%. This means that L is not sensitive to traffic conditions but very sensitive to the OD matrix in free-flow. Fig. 1c and d respectively present the evolution of the mean travel distance L_1 and L_2 related to routes R_1 and R_2. They show that L_1 and L_2 values are different but nearly constant in free-flow, i.e. when

n is below 90 veh when τ is close to 100% and R_1 and n below 50 veh when τ is close to 0% and R_2. This is due to the particular design of this network where the distance between local origins and local destinations are identical whatever the route choices are. The outflows for all local destinations are equal in free-flow to the inflows to these destinations. Furthermore, the total demand is uniformly distributed to the different origins and then to the destinations. All flows between local origins and destinations are thus identical. The mean travel distance for a given macroscopic route is constant because both local path lengths and flows have same values.

In congestion, a wide range of different values is observed for L, L_1 and L_2. This is because the outflows to each particular destination are no longer equal to the inflows but depend on the capacity settings and also on how the congestion has spread over the network. For example, higher L_1 values mean that $d_{1,1}$ is able to serve a higher flow than $d_{1,2}$ while lower L_1 values correspond to the reverse situations. In fact, the travel distances to $d_{1,1}$ are always higher than those to $d_{1,2}$. This explains why the results appear so scattered and why clear trends can not always be exhibited. This is both related to traffic conditions but also the OD matrix because the demand pattern influences the way congestion evolves in the network.

The main conclusion here is that the commonly used assumption about constant mean travel distance within a reservoir is not always true. It clearly depends on (i) internal traffic conditions within the reservoir and on (ii) the external OD matrix. It is important to mention that (ii) can also influenced (i), notably because it has a direct impact on how heterogeneous the network is. We will see in the next section that considering a single value for L leads to significant errors when calculating a key macroscopic variable, the total outflow Q.

2.3. Sensitivity of the outflow estimation to the mean travel distance

Usually for aggregate traffic modeling, the production is provided by the MFD and the outflow at the perimeter is derived from $Q=P/L$. It is then interesting to investigate the sensibility of Q to the errors on L. Tab. 1 presents eight methods, labeled m1 to m8, for estimating L on a macroscopic basis considering several layers of refinements in the reservoir description. Fig. 2 shows the sensitivity of the outflow to the estimation methods. For each simulation run, we compare the effective outflow with the ratio between the effective production and the estimation of L. This allows us to only focus on this last parameter.

Tab. 1. Definition of the different methods for calculating the travel distance L; $E(.)$ is the mathematical expectation (mean) for all runs; α is the effective fraction of the outflow that goes to D_1.

Method label	Route lengths (L_1 & L_2)	OD Matrix (τ)	Traffic conditions (n)	Calculation method
(m1)				$L=E(L)$
(m2)	✔			$L=\alpha E(L_1)+(1-\alpha)E(L_2)$
(m3)		✔		$L=E(L\|\tau)$
(m4)	✔	✔		$L=\alpha E(L_1\|\tau)+(1-\alpha)E(L_2\|\tau)$
(m5)			✔	$L=a\,n+b$
(m6)	✔		✔	$L=\alpha(a_1 n+b_1)+(1-\alpha)\,(a_2 n+b_2)$
(m7)		✔	✔	$L=a_{\|\tau}\,n+b_{\|\tau}$
(m8)	✔	✔	✔	$L=\alpha(a_{1\|\tau}\,n+b_{1\|\tau})+(1-\alpha)\,(a_{2\|\tau}\,n+b_{2\|\tau})$

Fig. 2a&b present the results for static methods (m1 to m4) that do not account for the traffic conditions. The simplest method m1 considers L as constant and equal to its mathematical expectation $E(L)$ whatever the OD matrix is. The blue dots in Fig. 2a show that the relative errors for the outflow are between -25% and 20%. These errors can lead to high deviation when using a MFD simulation model. However, we should mention that we consider here an extreme case because the OD matrix dramatically changes from one macroscopic destination to the other when τ varies from 0 to 100%. Red dots in Fig. 2a correspond to method m2 that takes advantage of the mean travel distances $E(L_1)$ and $E(L_2)$ for each macroscopic routes R_1 and R_2. The balance between both routes when calculating L is realized using the effective fraction α of the outflow that goes to D_1. In practice, we should estimate this fraction using for example the relative accumulation to D_1. Here, we use the exact partial outflows because we firstly focus on the errors related to L, L_1 and L_2. It appears that introducing the travel distances related to macroscopic routes reduces the errors when calculating the total outflow. However, these errors remain between -10% and 20%. This is

not surprising because the previous section shows that the OD matrix has a strong influence on the L, L_1 and L_2 values. A bias is observed for m2 in Fig. 2a. This is because L_i and Q_i values are not independent. The bias corresponds to the omission of the covariance terms when calculating L from L_1, L_2 and α.

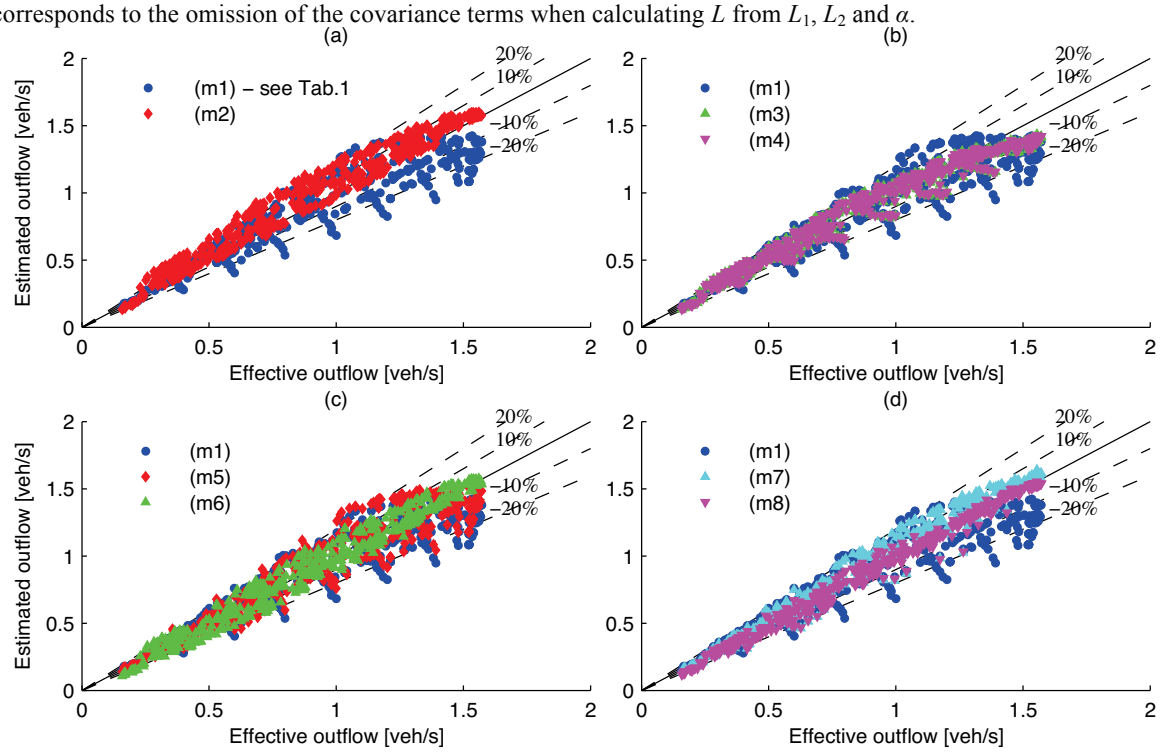

Fig. 2. Comparison between the effective outflow and the estimated outflow (P/L) using different calculation methods for L, see Tab. 1.

Fig. 2b investigates more precisely the role of the OD matrix. Now, $E(L)$, $E(L_1)$ and $E(L_2)$ are conditionally calculated given τ, see m3 (green dots) and m4 (pink dots) in Tab. 1 and Fig. 2b. The errors on the outflow are now between -10% and 10%. This clearly shows that the estimation of L should be updated when the demand pattern is considerably modified. This also indicates that considering only the demand pattern is not sufficient because the errors are not negligible. Note that there is no clear improvement here when the macroscopic routes are introduced (m4). This is because τ already segregates the traffic behavior on the macroscopic routes for this simple network.

Fig. 2c&d highlight the influence of traffic conditions (methods m5 to m8). We resort to the same distinctions between the estimation methods for L, i.e. with or without considering the macroscopic routes and with or without conditional calculations given τ but we add a third dimension, which is the influence of n. For the sake of simplicity, we chose linear approximations even if the relations between L, L_1 and L_2 may be more complex, see section 2.2. The idea here is to simply even roughly account for the trend of the evolution of L with respect to n. Fig. 2c shows that a single linear regression between L and n is not sufficient to improve the outflow results (red diamonds related to m5). This is not surprising because the linear approximation is not really relevant in that case, see Fig. 1c. Introducing the linear regression at the route level leads to much better results, see green triangles related to m6 in Fig. 2c. The results are even better than for m2, which also distinguishes the macroscopic routes but in a static context (red dots in Fig. 2a). This means that the most influential factor is the OD matrix or more precisely the OD flow distribution among routes but that the traffic conditions within the network also play a role. This is confirmed by Fig. 2d. Now, linear regressions with respect to n for L, L_1 and L_2 are performed after partitioning the runs with respect to τ. It appears that segregating the OD matrix clearly improves the outflow results. The best results for all methods are obtained with m8 when the conditional linear approximations are derived for each macroscopic route given τ, see pink dots in Fig. 2d. In that case, the 90% of the dots experiment errors between -5 and 5%.

This section does not aim to provide final conclusions on the best way to estimate L when calculating the total outflow but to identify the relevant factors. The first factor is the OD matrix when it experiments large variations. The second factor is the traffic conditions within the network. This section also shows that segregating the reservoir into macroscopic routes that clearly have different behavior in terms of travel distance helps to lower the errors on the outflow.

2.4. Sensitivity of the MFD shape to the OD matrix and the internal traffic conditions

In this section, we investigate how the OD matrix and internal traffic heterogeneities influence the shape of the MFD. In fact, the MFD and the outflow are the two key elements when studying the macroscopic traffic dynamics. Fig. 3a presents the evolution of the mean speed V with respect to n for all simulation runs. It appears that the MFD in speed is relatively well defined even if the OD matrix experiments contrasted demand patterns. A partial explanation should be related to the Wardrop's route choice model. Because the length between alternative local routes is always the same in this particular network, assigning vehicles in order travel times on alternative routes be close will lead to similar mean travel speeds. However, the OD matrix is far from playing no role. First, for a given n, the mean speeds fluctuate within a band of 1 to 2 m/s. This corresponds to a relative difference around 8% in free-flow but close to 50% for more severe congestion (n>150). Second, if the OD matrix would have no influence, the speed should be the same for a given n whatever the division over n_1 and n_2 is. Fig. 3b shows the speed contour plots with respect to n_1 and n_2. It appears that these contours are close to be lines at least when the repartition between n_1 and n_2 is not too contrasted, i.e. far from the axes. However, the slopes of these lines are between -0.6 and -0.8 and not close to -1 as expected if the mean speed would have been not sensitive to the repartition of vehicle among the macroscopic routes. Here the plots are not fully symmetric with respect to the first bisector. This means that if the OD matrix seems to have less influence on the mean speed than on the mean travel distance, this influence remains significant especially for contrasted scenario, i.e. low or high values of τ. A final proof is provided in Fig. 3c. The blue curve corresponds to the best fit of V with respect to n using a 3rd order polynomial expression. The red dots correspond to the best fit if we add as a second explanatory variable the fraction $r_1=n_1/n$ corresponding to the number of vehicle on route 1. A 1st order approximation is used for this variable. The r-square of both fits are above 0.98 which means good agreement for both and the sum of squared errors reduces from 163 to 143 m^2/s^2 when the second explanatory variable is considered. One more time, this mean that the flow distribution among routes is not of highest influence but cannot be fully neglected because it explains a part of the dispersion of the speed values for the same n.

Now, we will investigate the influence of internal heterogeneities on the shape of the MFD in speed. Previous works, e.g. (Geroliminis and Sun, 2011; Mazloumian *et al.*, 2010; Knoop *et al.*, 2013), suggest that the standard deviation s_k of the density over internal links is a good measure for network heterogeneity. So, we have also monitored this last variable when performing the simulation runs. Fig. 3d shows that s_k first linearly increases with n in free-flow and light congestion and then that s_k values are much more scattered. This means that very different situations in terms of network heterogeneities can be observed for the same n during heavy congestion. Those observations are in line with previous studies, e.g. (Mahmassani *et al.*, 2013). We chose a quadratic interpolation s_k^f to get a simple relation between s and n, see Fig. 3d. Then, we define the residual standard deviation $s_k'=s_k-s_k^f(n)$. We do this transformation because we want to introduce when fitting the V plots a second explanatory variable that characterizes the level of heterogeneity. From a statistical point of view, we should better introduce a variable that does not clearly depend on the first one. The red dots in Fig. 3e show the fit when a 3rd order polynomial approximation is used for n and a 1st order approximation is used for s_k'. The SSE is now reduced from 163 to 108 m^2/s^2 compared to the fit when only n is considered. The improvement is much better than when r_1 is used as a second explanatory variable, see Fig. 3c. This means that the internal traffic conditions and more precisely the level of heterogeneity has a higher impact on the scattering observed in the MFD in speed than the OD matrix. However, the OD matrix can be one of the source for the differences in the residual standard deviation s_k' for a given n.

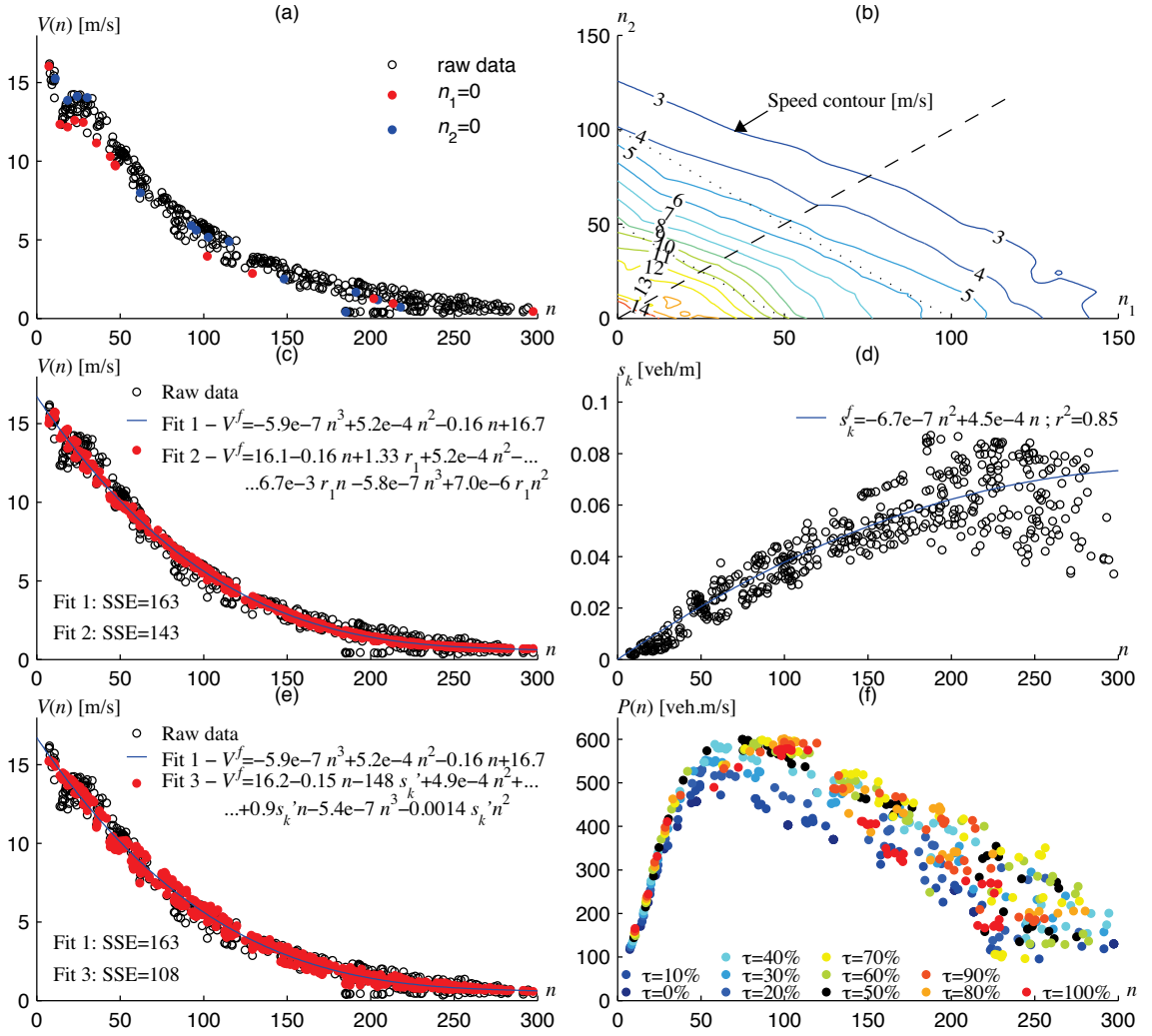

Fig. 3. (a) Mean speed V with respect to n; (b) V-Contour plots with respect to n_1 and n_2; (c) V-fits with respect to (i) n and (ii) n and the fraction r_1 of vehicles to D_1; (d) Standard deviation s of the density over internal links with respect to n; (e) V-fits with respect to (iii) n and the residual standard deviation s' of the density over links; (f) Production P with respect to n.

Finally, Fig. 3e presents the shape of the MFD in production. Recall that $P=nV$. The plots appear much more scattered than the MFD in speed for the congested part. This is only because the production magnifies the speed variations when n is high. In fact, we previously mentioned that the relative differences for the speed observations when n>150 can be in the order of 50% for a given n. A practical result here is that the MFD should better be fitted in speed than in production under strong heterogeneity. A final interesting result in this figure is that the maximum production and the bounds for the critical accumulations (n values where the production is maximal) appear to depend on τ. The lower bound for the critical accumulation is around 50 veh when τ=0% and around 100 veh when τ=100%. In the first case, all vehicles want to go to the south and the vertical links are the most crowded. In the second case, the reverse situation (to the east and horizontal links) is observed. Because, the horizontal links are longer (250 m) and more numerous (6) than the four vertical links (100 m), the capacity is reached for lower n values in the first case.

3. Multi-routes macroscopic model for reservoirs

Section 2 shows a particular network example where the OD matrix has a significant influence on the macroscopic traffic states. It is the first source of variations for the mean travel distance before the internal traffic conditions. It can also influence the MFD shape to a lesser extend. This should be considered with care when calibrating the MFD or the mean travel distance, in particular for the further use in a simulation model.

The current standard for simulation with MFD is a reservoir with a uniform perimeter and a single accumulation value. This framework cannot readily account for the impacts of the OD matrix on the macroscopic traffic variables and notably the difference in travel distances between some directions within the reservoir. In this section 3, we propose a new modeling framework to provide a better description of traffic dynamics when route patterns are heterogeneous. This framework also provides a more accurate description of the traffic wave propagation between macroscopic origins and destinations.

In this paper we only focus on traffic dynamics within a single reservoir. The problem of exchanging flows between reservoirs to simulate a whole city has already been tackled in several papers, e.g. (Geroliminis and Daganzo, 2007; Aboudolas and Geroliminis, 2013; Knoop and Hoogendoorn, 2014; 2015; Yildirimoglu and Geroliminis, 2014). The last two references account for origins and destinations when coupling the reservoirs and introduce a dedicated traffic assignment model.

3.1. Classical formulation with uniform reservoir

Classically, traffic dynamics within a reservoir is described at an aggregate level by the following conservation equation, e.g. (Geroliminis and Daganzo, 2007; Haddad *et al.*, 2013; Aboudolas and Geroliminis, 2013; Knoop and Hoogendoorn, 2014):

$$\frac{dn(t)}{dt} = q_{in}(t) - q_{out}(t) + d(t) \tag{1}$$

where q_{in} and q_{out} are respectively the inflow and the outflow at the reservoir perimeter and d is the net-inside flow corresponding to trips that start or end within the reservoir. The travel distance between any entry and exit points is constant and equal to L. Here, we are interested in how traffic waves propagate between the reservoir frontiers. Interestingly, (1) without the term d has already been extensively studied for link traffic dynamics in the so-called exit-flow models (Merchant and Nemhauser, 1978; Friesz, 1989). When the outflow is bounded by the supply of the neighboring link, it also corresponds to the discretized version of the LWR model (Lighthill and Whitham, 1955; Richards, 1956) in Eulerian coordinates (Daganzo, 1994; Lebacque, 1996) with one cell per link. Applied with discrete time-steps, such a formulation has been proved to be very diffusive (Carey and McCartney, 2004). Wave speeds can also be misestimated even if space and time are tuned to tightly fit the CFL condition.

Fig. 4 aims to illustrate the impacts of numerical viscosity within a reservoir (L=500 m) for two typical cases. The MFD in speed is assumed bilinear with a constant free-flow value equal to 20 m/s and then a decreasing branch between n_0 and $n_{\max}$, see Fig. 4a. The initial accumulation in the reservoir is n_b=50. Case 1 corresponds to a drop of the upstream demand at t=0 with an upstream accumulation state equal to n_a=10. Case 2 represents a congestion that reaches the reservoir downstream frontier also at t=0, see Fig. 4b. The downstream accumulation state is equal to n_c=120 in that latter case. Traffic flow theory tells us that shockwaves should be observed in both cases. The wave propagates from upstream to downstream in case 1 and in the reverse direction in case 2. The calculation of the analytical solution is straightforward, see Fig. 4b. Fig. 4c (respectively Fig. 4d) shows the outflow (respectively the inflow) numerically derived from equation (1) using the Godunov scheme (Godunov, 1959; Lebacque, 1996) for case 1 (respectively case 2). A single cell is used for the whole reservoir and two different time steps are tested Δt=1 and 28 s. These figures clearly highlight the effects of numerical viscosity even if the CFL condition is tight (Δt=28 s). The outflow in case 1 and the inflow in case 2 start decreasing before the waves should be noticed at the reservoir frontiers. Furthermore, the time required for the numerical solution to converge to the analytical one is very important (about 50 s). The effects worsen when the time step is reduced to 1 s.

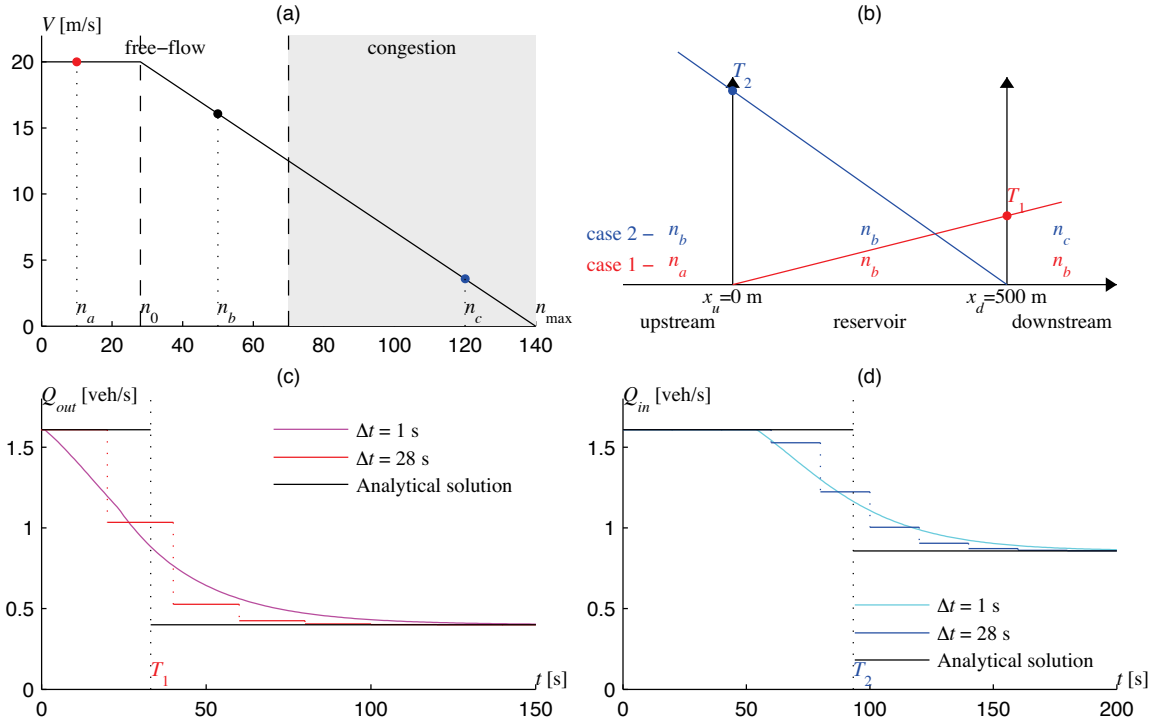

Fig. 4. (a) MFD in speed; (b) Two classical Riemann problems: upstream demand (case 1) and downstream supply (case 2) restrictions; (c) Outflow evolution for different time steps and case 1; (d) Inflow evolution for different time step and case 2.

A solution to get proper wave propagation within the reservoir is to explicitly account for the internal travelling distance when formulating the conservation equation. This transforms (1) to (2).

$$\frac{dk(x,t)}{dt} + \frac{\partial q(x,t)}{\partial x} = d(x,t) \quad \Leftrightarrow \quad \frac{dn(x,t)}{dt} + \frac{\partial P(x,t)}{\partial x} = D(x,t) \tag{2}$$

where x is the internal distance travelled, $k=n/L$ the internal density, q the internal flow and $d(x,t)$ (respectively $D(x,t)$) the net-inside flow (respectively production) that should now be localized with respect to x. (2) corresponds to the classical conservation equation used for link traffic dynamics (Lighthill and Whitham, 1995; Richards, 1956). Lots of efficient numerical schemes can be used to solve (2). Here we only mentioned those derived from the variational theory that are exact under some conditions (Daganzo, 2005; Mazaré *et al*, 2011).

The key idea here is to introduce a two layers process when simulating the behavior of reservoirs. The internal reservoir dynamics is explicitly considered by introducing the travelling distance x between 0 and L in (2) and a dedicated numerical scheme. This ensures proper internal wave propagation. Then, boundary flow at $x=0$ and $x=L$ are calculated and connected to other reservoirs using classical methods for aggregated traffic modeling (Knoop and Hoogendoorn, 2014; 2015; Yildirimoglu and Geroliminis, 2014). The main difference with link traffic dynamics is that L may change during the simulation (the link lengths in a network are fixe). We will see in the next section how (2) can be extended to account for multiple routes within a reservoir.

3.2. Introducing a new modeling framework with multiple macroscopic routes

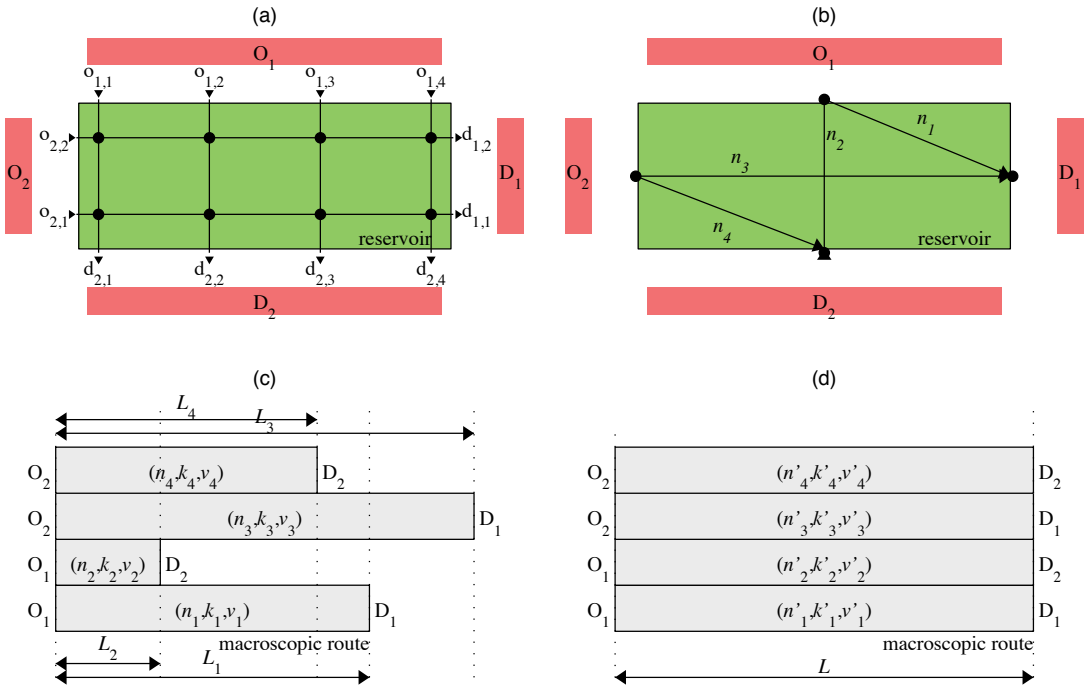

Fig. 5. (a) Complete network representation; (b) Network aggregated representation: the multi-routes reservoir concept; (c) Parrallel routes within the reservoir; (d) Parallel routes with a common spatial reference.

A reservoir provides an aggregated picture of the related network, see Fig. 5a. To define an intermediate level that distinguishes several macroscopic routes, the basic idea is to split the reservoir perimeter into several sub-regions that define the macroscopic origins (O) and destinations (D). Such macroscopic origins or destinations respectively gather several local origins (o) or destinations (d) that correspond to the effective network entries or exits, see Fig. 5a&b. The total number of vehicles n within the reservoir is then decomposed into a partial number of vehicles n_i for each macroscopic OD pair, see Fig. 5b. The mean travel distance L_i for each OD pair i can be individually set up and adjusted to the real observed values. Note that this concept of macroscopic route does not aggregate physical links but OD flows between all local origins and destinations that compose an OD pair. The correlation between different OD traffic states is defined by the MFD.

To our best knowledge, only (Yildirimoglu and Geroliminis, 2014) provides a framework with different travel distance per OD pair. However, it resorts to (1) for each partial flow and the wave propagation cannot be perfectly well represented within reservoirs. We are instead going to base our multi-route framework on equation (2) to introduce a refined description of wave propagation. We see in section 2.4 that the OD matrix has less influence on the MFD shape than on the travelling distance. Thus, we assume here that a well-defined MFD in speed can be exhibited for the reservoir and that it only depends on the total accumulation, i.e. $V(n)$. Furthermore, we also consider that L_i values are constant during the full simulation duration. We will discuss in section 4 how these two assumptions can be relaxed.

Let k_i, q_i, P_i, and v_i be respectively the density, the flow, the travel production and the speed related to the OD pair i. The conservation equation on the macroscopic route i including all the network paths from O to D is given by:

$$\frac{\partial k_i}{\partial t} + \frac{\partial k_i v_i}{\partial x_i} = d_i(x_i,t) \quad \forall i \tag{3}$$

where x_i is the curvilinear position along route i. Traffic dynamics within the reservoir can then be described by a system of parallel routes with different lengths, see Fig. 5c. Speeds in all routes are identical and given by the MFD, i.e. $v_i=V(n)$. A significant difference with existing approach based on uniform reservoir is that n explicitly depends on the internal travel distance because traffic states can evolve within the reservoir. Note that x_i is different for all routes because routes have different lengths. A common spatial reference can be adopted for all the routes by applying the following transformation: $x'_i=\varepsilon_i x_i$ where $\varepsilon_i=L/L_i$ and $L=\max(L_i)$. In the new referential, all routes have the same length $L'_i=L$. Other macroscopic variables are given by $n'_i=n_i$, $k'_i=k_i/\varepsilon_i$, $q'_i=q_i$, and $v'_i=\varepsilon_i v_i$, see Fig. 5d. This notably ensures that the travel-time for each route is not modified by the spatial transformation.

Finally, the traffic dynamics in the reservoir is defined by the following system of hyperbolic equations:

$$\frac{\partial k'_i}{\partial t} + \frac{\partial k'_i \varepsilon_i V(n')}{\partial x'_i} = d_i\left(x'_i,t\right) \quad \forall i \tag{4}$$

Some mathematical operations can be applied to exhibit the system conservative form:

$$\frac{\partial k'_i}{\partial t} + \varepsilon_i V(n')\frac{\partial k'_i}{\partial x'_i} + \varepsilon_i k'_i \frac{dV(n')}{dn'}\frac{\partial n'}{\partial x'_i} = d_i\left(x'_i,t\right) \quad \forall i$$

$$\Leftrightarrow \frac{\partial k'_i}{\partial t} + \varepsilon_i V(n')\frac{\partial k'_i}{\partial x'_i} + \varepsilon_i k'_i \frac{dV(n')}{dn'} L\sum_i \frac{\partial k'_i}{\partial x'_i} = d_i\left(x'_i,t\right) \quad \forall i$$

The conservative form of the system is then:

$$\frac{\partial K'}{\partial t} + A\frac{\partial K'}{\partial x'} = d \; ; A = \begin{pmatrix} \beta_1 & -\alpha_1 & \cdots & \cdots & -\alpha_1 \\ -\alpha_2 & \beta_2 & -\alpha_2 & \cdots & -\alpha_2 \\ \vdots & \cdots & \ddots & \cdots & \vdots \\ \vdots & \cdots & \cdots & \ddots & \vdots \\ -\alpha_n & \cdots & \cdots & -\alpha_n & \beta_n \end{pmatrix} ; \begin{matrix} \alpha_i = -\varepsilon_i n'_i \Upsilon(n) \\ \beta_i = \varepsilon_i\left(V(n) + n'_i \Upsilon(n)\right) \\ \Upsilon(n) = \dfrac{dV(n)}{dn} \end{matrix} \tag{5}$$

where $\boldsymbol{K}'$ is the vector $[k'_i]$, $\boldsymbol{d}$ is the vector $[d_i]$. Interestingly, system (5) that introduces multiple routes within a reservoir is similar to the system originally proposed in (Benzoni and Colombo, 2003) for multiclass traffic in a link. Indeed, in the new referential all macroscopic routes have the same length L but different speed v'_i that depends on the ratio ε_i between L and L_i.

System (5) has been extensively studied both in the mathematical and traffic flow literatures, e.g. (Wong and Wong, 2002; Zhang *et al.*, 2003; 2006; 2008; Herty *et al.*, 2008; Jin, 2012). Such a system is well-posed if it is hyperbolic (Leveque, 1992). This ensures that the solutions continuously depend on the initial conditions and that wave propagation is finite and well-defined. Mathematically speaking, system (5) is hyperbolic when all eigenvalues of A are real and when there is a complete, linearly independent set of eigenvectors. The analytical proof for (5) to be hyperbolic at least almost everywhere can be found in (Benzoni and Colombo, 2003) when $V(n)$ is linear without any restrictions on the dimension of n. This proof can be easily extended for bilinear relation with a constant initial step like in Fig. 4a. For more general and non-linear cases, (Zhang *et al.*, 2003) numerically verify that system (5) is

hyperbolic when the fundamental diagram in flow is concave. Here, we should translate this requirement to concave MFD in production or in flow.

3.3. A simple numerical scheme for the multi-route model

To run simulations including multi-route reservoirs, we need a numerical scheme to derive the internal traffic dynamics. The simplest numerical scheme for system like (5) is the Lax-Friedrichs scheme (Wong and Wong, 2002; Benzoni and Colombo, 2003). However, this scheme is known to be very diffusive. That is why higher order schemes like weighted essentially non-oscillatory (WENO) schemes have been proposed (Zhang *et al.*, 2003, 2006, 2008). Such schemes appear very efficient to reproduce shockwaves for multi-class traffic applications but they are quite complex to implement. We do not look here for a detailed description of the internal traffic dynamics but for a proper representation of wave propagation between the reservoir frontiers and for accurate calculations of the boundary flows (inflows and outflows for all macroscopic routes). That is why we propose to resort to the first order Godunov scheme (Godunov, 1959) combined with the Harten-Lax-van Leer (HLL) Riemann Solver (Harten *et al.*, 1983). To the author's best knowledge, this combination has never been applied to multiclass traffic. It appears in our context very efficient while simple. In this section, we will skip the source term $\boldsymbol{d}$ in (5) because numerically speaking accounting for source terms only implies to add or remove vehicles at specific locations.

The internal travelling distance L within the reservoir is first discretized into J cells of size Δx. These cells have less physical interpretation as for link traffic flow but they permit to properly track wave propagation between the reservoir frontiers x=0 and x=L. The density $k_{j,i,t}$ is updated at each time step Δt. j is the label of the cell, i the label of the OD pair and t the label of the time step. The total numbers of OD pairs and time steps are respectively I and T. The simulation duration is $T\Delta t$. The Godunov scheme provides the update procedure for all partial densities depending on the partial exit flows $q_{j\text{-}1,i,t}$ and $q_{j,i,t}$ of cells j and j-1 between times $t\Delta t$ and $(t+1)\Delta t$:

$$k_{j,i,t+1} = k_{j,i,t} + \left(q_{j-1,i,t} - q_{j,i,t}\right)\frac{\Delta t}{\Delta x} \tag{6}$$

The key point is the calculation of the partial exit flows between two successive cells. For first order hyperbolic equation (I=1), the exit flow in the Godunov scheme is given by the analytical solution of the Riemann problem defined by two successive cells. A Riemann problem corresponds to two successive steps of constant initial density. Here, we have to solve a multidimensional Riemann problem with I partial density values on both sides, see $\boldsymbol{N}_{\mathbf{U}}$=$(n_i)_{\mathrm{L}}$ and $\boldsymbol{N}_{\mathbf{D}}$=$(n_i)_{\mathrm{R}}$ in Fig. 6a. This is only possible when I is low and in practice for system (5) when I=2 (Benzoni and Colombo, 2003). For example, Fig. 6a shows the generic shape of the analytical solution when I=2. Two families of waves (1-waves and 2-waves) that can be either shockwave or rarefaction fan are successively observed from upstream to downstream. These wave speeds can be either positive or negative. An intermediate state $\boldsymbol{N}_{\mathbf{int}}$ is then observed. The readers are referred to (Leveque, 1992; Zhang, 2001; Benzoni and Colombo; 2003) for a complete description of the analytical solutions of Riemann problems for hyperbolic systems. When I is higher than 2, I wave families and I-1 intermediate states are observed. The analytical solution is no longer tractable. We will then resort to the HLL Riemann solver to approximate all the partial flows between two successive cells, i.e at x=x_0 see Fig. 6a.

The principle of the HLL approximate Riemann solver is the following (Toro *et al.*, 1994; Toro, 2009). Only the slowest and the fastest waves from all families are considered. Their speeds are respectively denoted S_{U} and S_{D}, see Fig. 6b. The approximate solution is composed of three partial density vectors from upstream to downstream: $\boldsymbol{N}_{\mathbf{U}}$ before the wave S_{U}, $\boldsymbol{N}_{\mathbf{HLL}}$ between S_{U} and S_{L} and $\boldsymbol{N}_{\mathbf{D}}$ after S_{D}. Let first assume that S_{U} and S_{D} are known. When S_{U} and S_{D} are both positive (respectively negative) the solution at x_0 is trivial and equal to $\boldsymbol{N}_{\mathbf{U}}$ (respectively $\boldsymbol{N}_{\mathbf{D}}$). The associated flow values $\boldsymbol{F}(\boldsymbol{N}_{\mathbf{U}})$ or $\boldsymbol{F}(\boldsymbol{N}_{\mathbf{D}})$ can then simply derived using the MFD: F_i=$(n_i/L_i)\mathrm{V}(n)$ for each OD pairs. Let now consider the case when S_{U} and S_{D} have opposite signs. In that case, we have to determine $\boldsymbol{N}_{\mathbf{HLL}}$ and the related partial flows. The HLL solver does this operation by applying the conservation principle twice, first on rectangle ABB'A' (7) and then on rectangle ACC'A (8), see Fig. 6b.

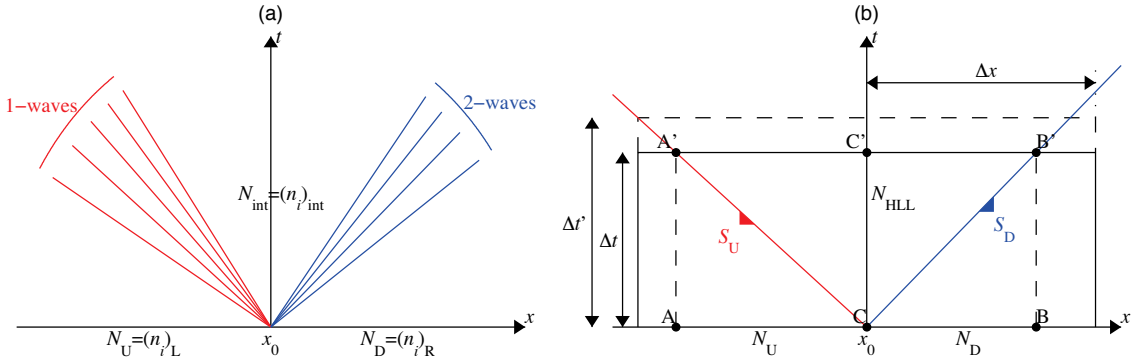

Fig. 6. (a) Generic representation for the analytical solution for 2 ODs; (b) HLL Riemann solver for the Godunov scheme.

$$\boldsymbol{N}_{\mathbf{HLL}}\left(S_{\mathrm{D}}\Delta t - S_{\mathrm{U}}\Delta t\right) = -\boldsymbol{N}_{\mathbf{U}}S_{\mathrm{U}}\Delta t + \boldsymbol{N}_{\mathbf{D}}S_{\mathrm{D}}\Delta t + F(\boldsymbol{N}_{\mathbf{U}})\Delta t - F(\boldsymbol{N}_{\mathbf{D}})\Delta t$$
$$\Rightarrow \quad \boldsymbol{N}_{\mathbf{HLL}} = \frac{\boldsymbol{N}_{\mathbf{D}}S_{\mathrm{D}} - \boldsymbol{N}_{\mathbf{U}}S_{\mathrm{U}} + F(\boldsymbol{N}_{\mathbf{U}}) - F(\boldsymbol{N}_{\mathbf{D}})}{(S_{\mathrm{D}} - S_{\mathrm{U}})} \tag{7}$$

$$-\boldsymbol{N}_{\mathbf{HLL}}S_{\mathrm{U}}\Delta t = -\boldsymbol{N}_{\mathbf{U}}S_{\mathrm{U}}\Delta t + F(\boldsymbol{N}_{\mathbf{U}})\Delta t - F(\boldsymbol{N}_{\mathbf{HLL}})\Delta t$$
$$\Rightarrow \quad F(\boldsymbol{N}_{\mathbf{HLL}}) = F(\boldsymbol{N}_{\mathbf{U}}) + S_{\mathrm{U}}(\boldsymbol{N}_{\mathbf{HLL}} - \boldsymbol{N}_{\mathbf{U}}) \tag{8}$$

By combining (7) and (8), we finally get:

$$F(\boldsymbol{N}_{\mathbf{HLL}}) = \frac{F(\boldsymbol{N}_{\mathbf{U}})S_{\mathrm{D}} - F(\boldsymbol{N}_{\mathbf{D}})S_{\mathrm{U}} + S_{\mathrm{D}}S_{\mathrm{U}}(\boldsymbol{N}_{\mathbf{D}} - \boldsymbol{N}_{\mathbf{U}})}{S_{\mathrm{D}} - S_{\mathrm{U}}} \tag{9}$$

The final expression for the vector of partial flows $\boldsymbol{F}$ between two cells with initial densities described by the vectors $\boldsymbol{N}_{\mathbf{U}}$ and $\boldsymbol{N}_{\mathbf{D}}$ is:

$$F = \begin{cases} F(\boldsymbol{N}_{\mathbf{U}}) & \text{if} \quad 0 \le S_{\mathrm{U}} \\ F(\boldsymbol{N}_{\mathbf{HLL}}) & \text{if} \quad S_{\mathrm{U}} < 0 < S_{\mathrm{D}} \\ F(\boldsymbol{N}_{\mathbf{D}}) & \text{if} \quad 0 \ge S_{\mathrm{D}} \end{cases} \tag{10}$$

To fully define the numerical scheme, the estimations of S_{U} and S_{D} are still missing. Usually, the absolute maximum for backward and forward wave speeds is used to tune S_{U}, S_{D} but also the CFL condition that ensures numerical stability and convergence for the scheme. Let λ_i be the eigenvalues of the matrix A in system (5) and $\lambda=\max(|\lambda_i|)$. Usually, explicit formulations for λ_i are hard to derive but global bounds can easily be identified. Then, $S_{\mathrm{U}}=-\lambda$, $S_{\mathrm{U}}=\lambda$ and $\Delta t=\Delta x/\lambda$ (tight CFL condition). Here, we propose to refine the estimation of S_{U} and S_{D} to improve the accuracy of the scheme. The idea is to adjust S_{U} and S_{D} to the initial conditions $\boldsymbol{N}_{\mathbf{U}}$ and $\boldsymbol{N}_{\mathbf{D}}$ for each pair of cells. We then look for local bounds for λ_i values. Local bounds per cell better capture local wave patterns than the usual global bounds. To this end, we apply the Gershgorin circle theorem (Gershgorin, 1931) to lines and rows of matrix A in (5):

$$\forall i \quad \left|\lambda_i - \beta_i\right| \le (I-1)\alpha_i \quad \text{(lines)}; \quad \forall i \quad \left|\lambda_i - \beta_i\right| \le \sum_{k \ne i} \alpha_k \quad \text{(rows)} \tag{11}$$

From (11) and by noticing that $n=\Sigma n_i$ and that $\Upsilon(n)$ (the derivative of $V(n)$ with respect to n) is always negative, we can derive the following expressions:

$$\forall i \quad \underbrace{\varepsilon_i V(n) + \Upsilon(n)\sum \varepsilon_k n_k}_{rows} \le \lambda_i \le \underbrace{\varepsilon_i \left(V(n) - (I-2)n_i \Upsilon(n)\right)}_{lines} \tag{12}$$

$$\begin{aligned} &\forall i \quad \varepsilon\left(V(n) + \Upsilon(n)\sum n_k\right) \le \lambda_i \le \varepsilon_i V(n) \ \text{ where } \varepsilon = \max(\varepsilon_i) \\ &\forall i \quad \varepsilon\left(V(n) + n\Upsilon(n)\right) \le \lambda_i \le \varepsilon V(n) \end{aligned} \tag{13}$$

It worth to mention that $V(n)+n\Upsilon(n)=(nV(n))'$ is the derivative of the MFD expressed as the total production with respect to n. Finally, the estimations of S_U and S_D for two consecutive cells with total density values equal to n_U and n_R are given by (13). Thanks to these estimations, we can also adjust the CFL condition at each temporal iteration. This speeds up the calculations. The time-step for iteration t is set to $\Delta t=\Delta x/\max(|S_{U,i}|,|S_{R,i}|)$.

$$S_U = \varepsilon \min\left(V(n_U) + n_U \Upsilon(n_U), V(n_L) + n_L \Upsilon(n_L)\right); \ S_D = \varepsilon \max\left(V(n_U), V(n_L)\right) \tag{14}$$

Fig. 7 presents four numerical examples, labeled from *a* to *b*, when $I=2$ and the MFD in speed is defined by Fig. 4a. The mean travel distance for both routes are $L_1=500$ m and $L_2=200$ m. We chose to discretize the reservoir length $L=500$ m into 80 cells, i.e. $\Delta x=6.25$ m. The initial conditions correspond either to changes in the upstream or the downstream traffic conditions. The initial n_i values are provided in Fig. 7_(1) and Fig. 7_(2) under brackets. These four examples highlight all the possible situations for both wave families, i.e. a shockwave or a rarefaction fan. Because $I=2$, we are also able to calculate the analytical solutions associated to all Riemann problems and then to easily assess the accuracy of the proposed numerical scheme. Fig. 7_(1)&(2) respectively presents the space-time diagram for the partial accumulations n_1 and n_2. Fig. 7_(3) the evolution of the partial and total flows at the reservoir frontiers (in- or outflows depending on the cases). This last graph is the most important in the context of macroscopic simulation because it corresponds to the flows that the reservoir will exchange with its neighbors.

Fig. 7 shows that the proposed numerical scheme is very accurate. Shockwaves are properly represented and the numerical solutions closely follow the analytical one. The total and partial outflows in Fig. 7a&b and inflows in Fig. 7c&d are exactly reproduced. The higher discrepancies are observed close to the borders of rarefaction fans, see for example Fig. 7a at $t=25$ s, Fig. 7b3 and $t=43$ s and Fig. 7c3 and $t=24$ s. However, the discrepancies remain negligible in all cases especially if we compare with what we observed in Fig. 4c&d. Introducing an explicit representation of the travelled distance within the reservoir clearly leads to accurate wave propagation. In these four cases, using adaptive time steps reduces by about 20% the number of iterations for the same simulation duration. Furthermore, we also test the numerical scheme with only 8 internal cells for the reservoir and we still obtain very satisfactory results compared to the analytical simulation.

3.4. A more complex test case with multiple routes

We now present a more complex test case with 4 macroscopic routes (2 origins and 2 destinations). This illustrates the model and the numerical scheme capabilities in a typical situation. The MFD in speed within the reservoir is set to the one observed in section 2, see Fig. 3c. The mean travel distances per OD are respectively 500, 200, 400 and 300 m. The reservoir is empty at $t=0$ s. The number of internal cells is again fixed to 80. A two-step demand profile is applied to the four macroscopic routes, see Fig. 8a. The network is first loaded with high demand values. The demands then decrease at time $t=250$ s. The downstream supply is not limited expect between times $t=250$ and $t=600$ s. This creates an internal congestion because the demand exceeds the supply. The congestion is able to reach the reservoir origins. After time t=600 s, the reservoir recovers to free-flow conditions because the supply is no longer limited. Fig. 8a provides under brackets the partial accumulation values for all boundary

conditions. Fig. 8c present the space-time within the reservoir for each partial accumulation n_i. Fig. 8b shows the time-evolution of the outflows for all macroscopic routes.

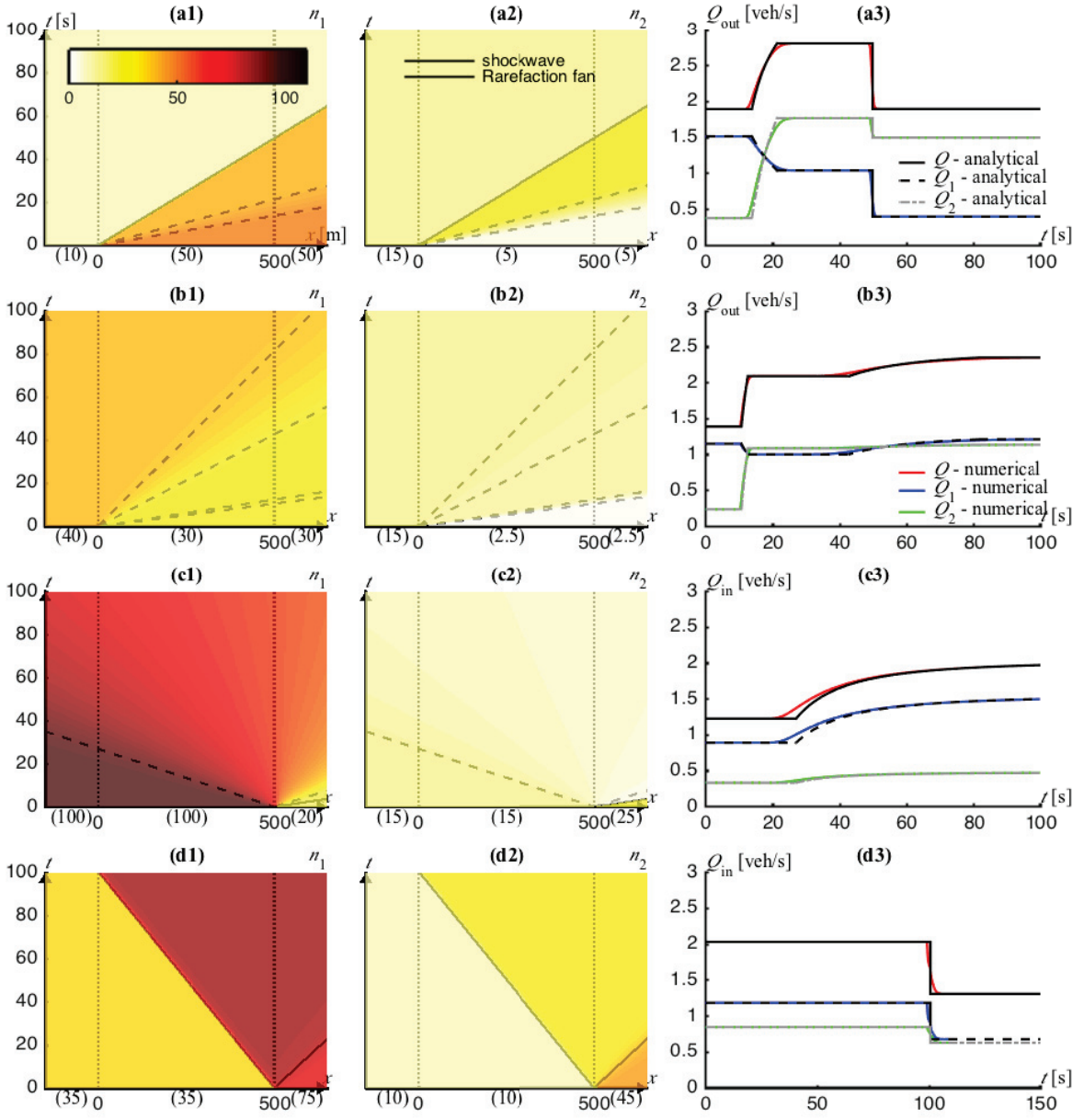

Fig. 7. Comparison between the analytical and the numerical solutions for 2 ODs. (a) 1-shock & 2-fan; (b) 1-fan & 2-fan; (c) 1-fan & 2-shock; (d) 1-shock & 2-shock; (1) Space-time diagram for n_1; (2) Space-time diagram for n_2; (3) Out- or inflow time-evolution at the reservoir frontiers.

It is no longer possible to assess the accuracy of the numerical scheme compared to the analytical solution. However, we can see in Fig. 8c that the waves are properly reproduced with little numerical diffusion. At the beginning of the simulation, each macroscopic routes reaches a full loading at different times, see Fig. 8b. This is exactly what we expect because the travel distances are different. Route 1 has the highest distance and its outflow is the last to reach the first demand step. When the congestion appears, all outflows are immediately bounded. A single

wave with same speed propagates from downstream to upstream within the reservoir. Because, the MFD only depends on n and not on the partial accumulation, as soon as a speed reduction appears at one of the macroscopic destination, it is automatically applied to all destinations. This may be seen as a limitation of the model but this can be overcome by refining the shape of the MFD. This will be discussed in the next section. A good point here is that the wave speed accounts for the flow distribution among routes and the differences in the travel distances. During the recovery phase (t>600 s), wee see that the flow evolutions are different with respect to the routes. The shortest route (R2) recovers first and then the others in ascending order of their travel distances. We observe fluctuations of the different outflows during this period because of the interactions between route flows that make different intermediate states appear. Finally, the reservoir stabilizes to the new demand values.

This example shows that the numerical scheme behaves well with more OD pairs. Wave propagation fits our expectation and the outflows properly account for the difference in travel distances. A general configuration for a reservoir would be 16 OD pairs (4 origins and 4 destinations, see Fig. 5b). We have performed some initial tests with such a configuration but the results can hardly be plotted.

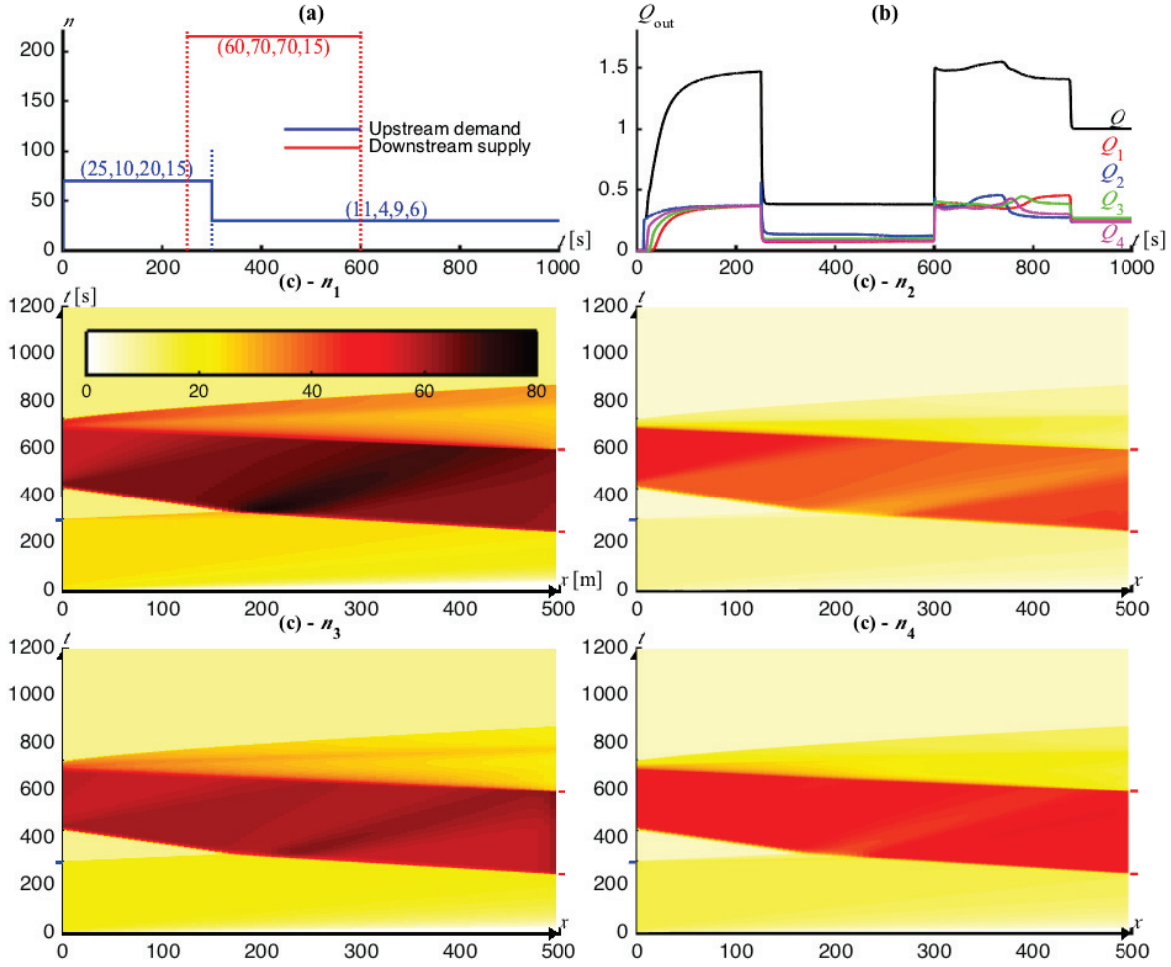

Fig. 8. Test case with I=4 (a) Demand and supply profiles; (b) Evolution of the total and partial outflows; (c) Space-time diagram within the reservoir.

4. Discussion

This paper shows that the OD matrix may have a significant influence on the macroscopic traffic dynamics related to a given road network. In particular, the mean travel distance is even more sensitive to this factor than to internal traffic conditions. The MFD shape can also be modified when different flow distributions are applied to the same network. A refined modeling framework has been presented in this paper to represent the reservoir internal dynamics. The idea is to partition the paths within a reservoir into several macroscopic routes where traffic dynamics are separately tracked. The first advantage is that the reservoir perimeter is no longer uniform because several macroscopic origins and/or destinations are identified. The second advantage is that routes with significantly different travel distances can be distinguished. The resulting framework proposes a better description of wave propagation between the reservoir upstream and downstream frontiers compared to existing approaches. It also permits a clear distinction of the flow directions between different parts of the reservoir perimeter. Numerical results have been obtained using a Godunov scheme combined with the HLL Riemann approximate solver. This combination provides accurate results in terms of wave propagation while remaining fast and simple in terms of computational implementation.

Several assumptions have been made in this paper when describing the new model for multi-route reservoirs. We considered that the mean travel distances per OD pair are constant over the full simulation duration and that the MFD in speed only depends on the total accumulation. These assumptions may appear restrictive compared to the observations made in section 2 or in other papers from the literature. We would like now to propose some guidance about how such assumptions can be relaxed.

With regards to the travel distances, the proposed framework can easily account for dynamic updates of L_i values. When L_i is updated, the accumulation n_i remains unchanged while the density k_i is modified. Shockwave theory tells us that jumps in density can easily be handled provided that the density values remain within their validity domain. Notably, a problem may be observed when L_i is reduced because k_i may then overtake its maximal bound. This means that L_i should only vary smoothly and enough slowly. In practice, it seems interesting to correlate L_i with n. In section 2, the variations of L_i with respect to n looks smooth with relatively low amplitude. Moreover, the variations are often well oriented (L_i values only decrease if n also decreases). Anyway, this question should be checked when calibrating the relations that describe the evolution of L_i. An interesting research question is to look for explicit expressions for such relations with respect to the network topology, signal settings and the local traffic assignment.

With regards to the MFD shape, it is possible to introduce refine expressions at a higher calibration cost. In section 2.4, two options have been investigated: V depends on all partial accumulations n_i, i.e. $V(n_1,\dots,n_I)$ or V depends on n and the standard deviation s of n over internal links, i.e. $V(n,s)$. The first option is more flexible and is able to account for specific evolution of the MFD related to drastic changes in the OD matrix. The second option is more parsimonious and has been proven to be relevant in different context, e.g. (Geroliminis and Sun, 2011; Mazloumian *et al.*, 2010; Knoop *et al.*, 2013). The main limitation of this last approach is that the inhomogeneity s_k can be easily measured from local network information but is hard to estimate only from a macroscopic perspective. The multi-route reservoir model can help to overtake this because it can provide a direct even rough estimation of s_k using the standard deviation of the partial accumulation n_i on macroscopic routes. Introducing refined expressions for the MFD will reduce the "one is all" effect when congestion appears at one destination. Indeed, when V only depends on n, the congestion is immediately experimented by all routes (but only at their ends) while we would have expected more nuanced interactions. The proposed numerical scheme can straightforwardly adapt to more refined MFD shape. However, deeper mathematical investigations would be required to guaranty that system (5) remains well-posed, i.e. hyperbolic, for the considered MFD.

A last advantage of the proposed modeling framework should be underlined: the explicit consideration of the internal distance travelled x. First, this permits to more precisely localize source terms within the reservoir, see term $d_i(x,t)$ in (3) and to refine the setting of the travel distance for trips that start or end within the reservoir. Furthermore, internal flows can be assigned to macroscopic routes and have their specific travel distances. In the classical reservoir representation, only their contribution to the total accumulation is taken into account. Second, internal bottlenecks (bridges, tunnels, specific intersections…) can simply be considered along routes and precisely localized. Hans *et al* (2014) shows for an urban corridor that identifying the most restricting capacity constraint along the route clearly improves the representation of macroscopic dynamics using MFD. The numerical scheme presented in this

paper is able to directly handle partial capacity constraints per route at each cell boundaries. This may pave the way to valuable extensions.

Further research directions investigated by the authors are (i) the effective introduction of more refined MFD shape within the reservoir (ii) the combination of the multi-route reservoir model with existing works for interfacing reservoir perimeters and then get a full simulation model for cities and (iii) the calibration of refined MFD shape as well as the relationship able to describe the variations of the mean travel distance on macroscopic routes.

Acknowledgements

This research has been partly funded by the French Research Agency (ANR) within the project TRAFIPOLLU (ANR-12-VBDU-0002). It is sponsored by a visiting researcher grant from the Delft University of Technology Transport Institute and the NWO grant "There is plenty of room in the other lane".

References

Aboudolas, K., Geroliminis, N., 2013. Perimeter and boundary flow control in multi-reservoir heterogeneous networks. Transportation Research Part B, 55:265-281.

Benzoni, S., Colombo, R., 2003. A n-populations model for traffic flow. European Journal of Applied Mathematics, 14:587-612.

Carey, M., McCartney, M., 2004. An exit-flow model used in dynamic traffic assignment. Computers & Operations Research, 31:1583-1602.

Daganzo, C.F., 2007. Urban Gridlock: Macroscopic modeling and mitigation approaches. Transportation Research Part B, 41(1):49-62.

Daganzo, C.F., 2005. A variational formulation of kinematic waves: basic theory and complex boundary conditions. Transportation Research Part B, 39(2): 187-196.

Daganzo, C., 1994. The cell transmission model: A dynamic representation of highway traffic consistent with the hydrodynamic theory. Transportation Research Part B, 28(4):269-287.

Friesz T.L., Luque, J., Tobin R.L., Wie, B.W., 1989. Dynamic network traffic assignment considered as a continuous time optimal control problem. Operations Research, 37(6):893–901.

Geroliminis, N., Haddad, J., Ramezani, M., 2013. Optimal perimeter control for two urban regions with macroscopic fundamental diagrams: a model predictive approach. IEEE Transactions on Intelligent Transportation Systems, 14(1):348–359.

Geroliminis, N., Sun, J., 2011. Properties of a well-defined macroscopic fundamental diagram for urban traffic. Transportation Research Part B, 45(3):605-617.

Geroliminis, N., Daganzo, C.F., 2008. Existence of urban-scale macroscopic fundamental diagrams: some experimental findings. Transportation Research Part B, 42(9):759-770.

Geroliminis, N., Daganzo, C., 2007. Macroscopic Modeling of Traffic in Cities #07-0413. Proceedings of the 88th Transportation Research Board Annual Meeting (TRB). Washington: Transportation Research Board, 16p.

Gerschgorin, S., 1931. Über die Abgrenzung der Eigenwerte einer Matrix. Izv. Akad. Nauk. USSR Otd. Fiz.-Mat. Nauk, 6:749–754.

Godfrey, J., 1969. The mechanism of a road network. Traffic Engineering and Control, 11(7):323-327.

Godunov, S.K., 1959. A difference scheme for numerical computation of discontinuous solutions of equations of fluid dynamics. Mat. Sb., 47:271-290.

Hans, E., Chiabaut, N., Leclercq, L., 2014. Application of the variation theory to travel time estimation on urban arterials, Transportation Research part B, *accepted for publication.*

Haddad, J., Ramezani-Ghalenoei, M., Geroliminis, N., 2013. Cooperative traffic control of a mixed network with two urban regions and a freeway. Transportation Research Part B, 54:17-36.

Harten, A.,Lax, P., van Leer, B., 1983. On upstream differencing and Godunov type methods for hyperbolic conservation laws. SIAM review, 25(1): 35-61.

Herman, R., Prigogine, I., 1979. A two-fluid approach to town traffic. Science, 204:148–151.

Herty, M., Kirchner, C., Moutari, S., Rascle, M., 2008. Multicommodity flows on road networks. Communications in Mathematical Sciences, 6(1): 171–187.

Hunt, P.B., Robertson, D.I., Bretherton, R.D., Royle, M.C., 1982. The SCOOT on-line traffic signal optimization technique. Traffic Engineering and Control, 23:190–192.

Ji, Y., Geroliminis, N., 2012. On the spatial partitioning of urban transportation network. Transportation Research Part B, 46(10):1639-1656.

Jin, W.L., 2012. A kinematic wave theory of multi-commodity network traffic flow. Transportation Research part B, 46(8): 1000–1022.

Keyvan-Ekbatani, M., Kouvelas, A., Papamichail, I., Papageorgiou, M., 2012. Exploiting the fundamental diagram of urban networks for feedback-based gating. Transportation Research Part B, 46(10):1393–1403.

Knoop, V.L. and Hoogendoorn, S.P., 2015. An Area-Aggregated Dynamic Traffic Simulation Model, European Journal of Transportation and Infrastructure Research - in press.

Knoop, V.L., Hoogendoorn, S.P., 2014. Network Transmission Model: a dynamic traffic model at network level. Proceedings of the 93rd Transportation Research Board Annual Meeting (TRB). Washington: Transportation Research Board, 21p.

Knoop, V.L., Hoogendoorn, S.P., 2013. Empirics of a Generalized Macroscopic Fundamental Diagram for Urban Freeways, Transportation Research Record, 2391, 133-141.

Knoop, V.L., Hoogendoorn, S.P., Van Lint, H., 2013. Impact of Traffic Dynamics on Macroscopic Fundamental Diagram #13-0595. Proceedings of the 92nd Transportation Research Board Annual Meeting (TRB). Washington: Transportation Research Board, 19p.

Kouvelas, A., Aboudolas, K., Papageorgiou, M., Kosmatopoulos, E., 2011. A hybrid strategy for real-time traffic signal control of urban road networks. IEEE Transactions on Intelligent Transportation Systems, 12(3):884–894.

Lebacque, J.P., 1996. The Godunov scheme and what it means for first order traffic flow models. In: Lesort J.B. (Ed.), 13th ISTTT, Pergamon, London, 647-678.

Leclercq, L., Becarie, C., 2012. A Meso Lighthill-Whitham and Richards Model Designed for Network Applications. Proceedings of the 91st Transportation Research Board Annual Meeting (TRB), 21-26 January, Washington, (USA) [CDROM]. Washington: Transportation Research Board, 10p.

Leclercq, L., Geroliminis, N., 2013. Estimating MFDs in simple networks with route choice. Transportation Research Part B, 57:468-484.

Leveque, R.J., 1992. Numerical methods for conservation laws. 2nd Edition. Bâle: Switzerland, Birkhäuser, 214 p.

Lighthill, M.J., Whitham, J.B., 1955. On kinematic waves II: A theory of traffic flow in long crowded roads. Proceedings of the Royal Society, A229:317-345.

Lowrie, P.R., 1982. SCATS: the Sydney co-ordinated adaptive traffic system – Principles, methodology, algorithms. In: Proceedings of the IEE International Conference on Road Traffic Signaling. London, England, 67–70.

Mahmassani, H.S., Hou, T., Saberi, M., 2013. Connecting Networkwide Travel Time Reliability and Network Fundamental Diagram of Traffic Flow. Transportation Research Records, 2391, 80-91.

Mahmassani, H.S., Williams, J.C., Herman, R., 1987. Performances of Urban Traffic Networks. In: (Gartner, N.H., Wilson, N.H.M., Eds) Proceedings of the 10th International Symposium on Transportation and Traffic Theory, 1-20.

Mahmassani, H.S., Williams, J.C., Herman, R., 1984. Investigation Of Network-Level Traffic Flow Relationships: Some Simulation Results. Transportation Research Record, 971:121-130.

Mazloumian, A., Geroliminis, N., Helbing, D., 2010. The spatial variability of vehicle densities as determinant of urban network capacity. Philosophical Transactions of Royal Society A, 368(1928):4627-4648.

Mazaré, P.E., Dehwah, A.H., Claudel, C.G., Bayen, A.M., 2011. Analytical and grid-free solutions to the Lighthill–Whitham–Richards traffic flow model. Transportation Research Part B, 45(10): 1727-1748.

Merchant DK, Nemhauser GL., 1978. A model and an algorithm for the dynamic tra(c assignment problem. Transportation Science, 12(3):183–199.

Richards, P.I., 1956. Shockwaves on the highway. Operations Research, 4:42-51.

Toro E F., 2009. Riemann Solvers and Numerical Methods for Fluid Dynamics: A Practical Introduction. Third Edition. Berlin: Springer-Verlag, 721 p.

Toro, E.F., Spruce, M., Speares, W., 1994. Restoration of the contact surface in the Harten-Lax-van Leer Riemann solver. Shock Waves. 4: 25-34.

Wardrop, J. G., 1952. Some theoretical aspects of road traffic research. Institution of civil engineers, 2, 325–378.

Wong, G.C.K., Wong, S.C., 2002. A multi-class traffic flow model – an extension of LWR model with heterogeneous drivers. Transportation Research part A, 36(9):827–841.

Yildirimoglu, M., Geroliminis, N., 2014. Approximating dynamic equilibrium conditions with macroscopic fundamental diagrams #14-0709. Proceedings of the 93rd Transportation Research Board Annual Meeting (TRB). Washington: Transportation Research Board, 19p.

Zhang, H.M., 2001. A finite difference approximation of a non-equilibrium traffic flow model. Transportation Research part B, 35(4):337–365.

Zhang, P., Wong, S.C., Xu, Z., 2008. A hybrid scheme for solving a multi-class traffic flow model with complex wave breaking. Comput. Methods Appl. Mech. Engrg. 197:3816–38.

Zhang, P., Wong, S.C., Shu, C.W., 2006. weighted essentially non-oscillatory numerical scheme for a multi-class traffic flow model on an inhomogeneous highway. Journal of Computational Physics, 212:739–756.

Zhang, P., Shu C.W., Wong, G.C.K., Wong, S.C., 2003. A weighted essentially non-oscillatory numerical scheme for a multi-class Lighthill–Whitham–Richards traffic flow model. Journal of Computational Physics, 191:639–659.